Lecture "Solid-State NMR Spectroscopy"

of the module „Structure Elucidation"

for Chemistry Bachelor students at the University Stuttgart

given by apl. Prof. Dr. Michael Hunger

until summer course 2020

"Solid-State NMR Spectroscopy" by apl. Prof. Dr. Michael Hunger:

1.   Introduction to Nuclear Spin Interactions in Solids

1.1   Survey on Nuclear Spin Interactions

- positions and shapes of solid-state NMR (SSNMR) signals are determined by the following nuclear spin interactions:

$$H_{total} = H_0 + H_Q + H_K + H_{DI} + H_{CSA} + H_J \qquad (1)$$

Hamiltonian	Description	Frequency / signal broadening
H_0	Zeeman interaction of the magnetic nuclear dipole moment μ_i with the magnetic B_0 field	$\leq 10^9$ s^{-1}
H_Q	interaction of the electric nuclear quadrupole moment of spin $I > \frac{1}{2}$ nuclei with electric field gradients at the position of the nuclei	$\leq 10^7$ s^{-1}
H_K	Knight shift due to the interaction of resonating nuclei with unpaired electrons in their neighbourhood	$\leq 10^5$ s^{-1}
H_{DI}	direct interaction of the magnetic dipole moment of the resonating nucleus with magnetic dipole moments of neighbouring nuclei	$\leq 5 \times 10^4$ s^{-1}
H_{CSA}	anisotropic chemical shielding σ due to the attenuation of the local B_0 field by the electron shell	$\leq 5 \times 10^3$ s^{-1}
H_J	J-coupling, scalar interaction or indirect nuclear spin-spin interaction caused by bonding electrons	$\leq 5 \times 10^2$ s^{-1}

1.2 Zeeman Interaction

- Hamiltonian $\boldsymbol{H}_0$ of the Zeeman interaction of nuclei with spin I and the gyromagnetic ratio γ_I in an external magnetic $\boldsymbol{B}_0$ field:

$$\boldsymbol{H}_0 = -\gamma_I \cdot \hbar \cdot \boldsymbol{I} \cdot \boldsymbol{B}_0 \tag{2}$$

- splitting of the nuclear energy levels according to their magnetic quantum numbers m (bottom, left)

- the transition frequency between these energy level corresponds to the Larmor frequency ν_0:

$$\nu_0 = \frac{\gamma_I}{2\pi} \, \boldsymbol{B}_0 \tag{3}$$

- in the classical picture, the Larmor frequency is the spinning frequency of the magnetic dipole moments μ_i (bzw. μ) on a cone-surface, which is directed along the $\boldsymbol{B}_0$ field (bottom, right)
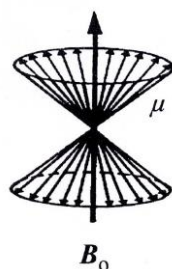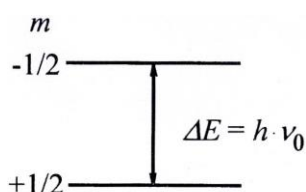
1.2 Quadrupolar Interaction

- nuclei with a spin $I > \frac{1}{2}$ are characterized by an elliptic charge distribution
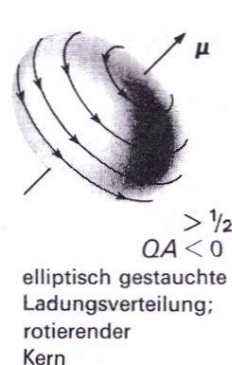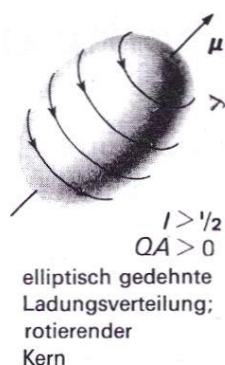
- this charge distribution causes a nuclear quadrupole moment eQ (proportional to the quadrupolar anisotropy QA in the top Figure)

Nucleus	^{2}H	^{23}Na	^{27}Al	^{41}Ca	^{241}Pu
Spin I	1	3/2	5/2	7/2	5/2
eQ	e × 0.29	e × 10.40	e × 14.66	-e × 6.70	e × 560

- for spins $I = 3/2, 5/2, 7/2$ etc., in addition to the central transition (-1/2 ↔ +1/2) also satellite transitions (z.B. -3/2 ↔ -1/2, +1/2 ↔ +3/2 etc.) exist

$$\Delta = (1/2)\omega_Q(3\cos^2\beta - 1)$$
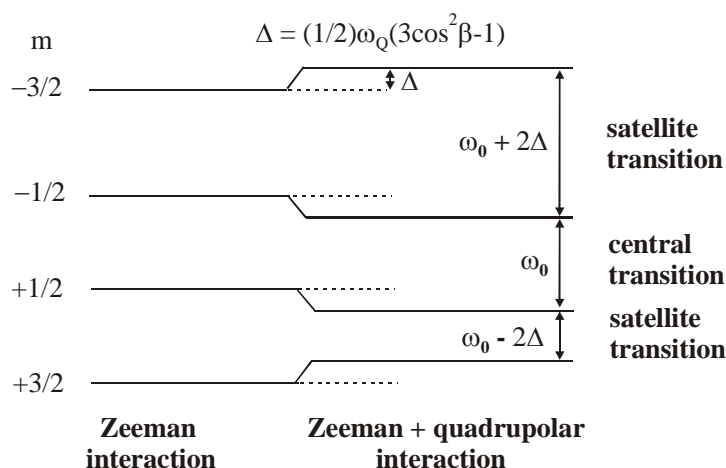
- the signal of the central transition occurs at the centre of gravity near ω_0
- satellite signals are shifted by $\pm 2\Delta$ relative to the central transition
- the value of Δ depends on the quadrupole frequency $\omega_Q = 2\pi\nu_Q$ as well as the angle β between the z direction of the electric field gradient $V_{zz} = eq$ at the position of the nucleus (parameter of local structure) and the B_0 direction

single crystal   powder sample
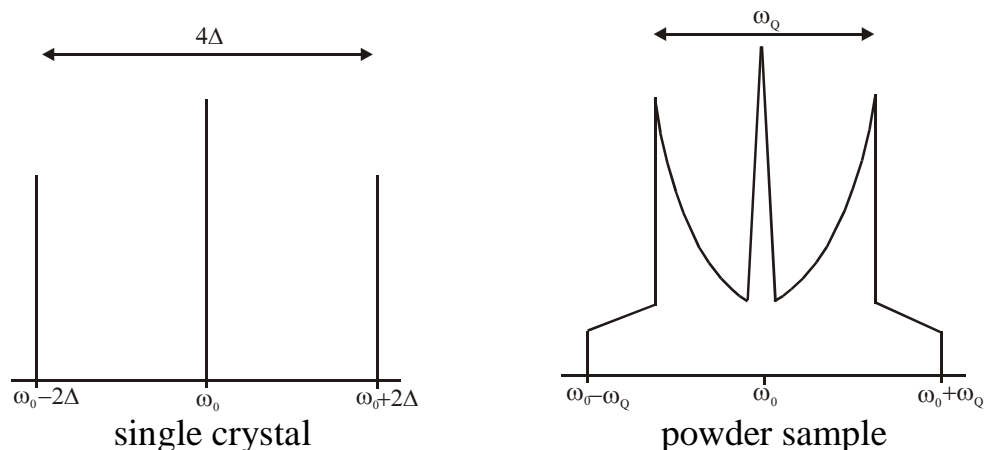
- relative signal intensities A of the central transitions (CT) and the satellite transitions (ST):

$$A(\text{CT,ST}) = \frac{3}{2}\frac{I(I+1)-m(m-1)}{I(I+1)(2I+1)} \tag{4}$$

transitions	ST	ST	ST	ST	CT	ST	ST	ST	ST
$I=1$				1/2		1/2			
$I=3/2$			3/10		4/10		3/10		
$I=2$		2/10		3/10		3/10		2/10	
$I=5/2$	5/35		8/35		9/35		8/35		5/35

(nuclei with spin I = 1, 2, 3 etc. have no central transition)

- Hamiltonian $\boldsymbol{H}_Q$ of the quadrupolar interaction:

$$\boldsymbol{H}_Q = \frac{e^2qQ}{4I(2I-1)}[3I_z^2-I(I+1)]\left(\frac{3\cos^2\beta-1}{2}+\frac{\eta_Q}{2}\sin^2\beta\cos2\alpha\right) \tag{5}$$

with asymmetry parameter η_Q and components of the electric field gradient V ($V_{zz} \geq V_{yy} \geq V_{xx}$):

$$\eta_Q = \frac{V_{xx}-V_{yy}}{V_{zz}} \tag{6}$$

and the Euler angles α and β between the principle axes of the electric field gradient tensor and the laboratory frame

- the quadrupole coupling constant C_q corresponds to the strength of the quadrupolar interaction (proportional to the product of eQ and $eq = V_{zz}$):

$$C_q = \frac{e^2qQ}{h} \tag{7}$$

- relationship between C_q and the quadrupole frequency $\omega_Q = 2\pi\nu_Q$:

$$\nu_Q = \omega_Q/2\pi = \frac{3e^2qQ}{2I(2I-1)h} = \frac{3C_q}{2I(2I-1)} \tag{8}$$

- frequency distribution function (signal shape) of the central transitions ($-1/2$ $\leftrightarrow +1/2$) of quadrupole nuclei [Freude1]:

$$\omega_{-1/2,+1/2} = -\frac{\omega_Q^2}{6\omega_0}\left[I(I+1)-\frac{3}{4}\right](A\cos^4\beta + B\cos^2\beta + C) \qquad (9)$$

with

$$A = -\frac{27}{8}-\frac{9}{4}\eta\cos 2\alpha -\frac{3}{8}\eta^2\cos^2 2\alpha \qquad (10)$$

$$B = +\frac{15}{4}-\frac{1}{2}\eta^2 + 2\eta\cos 2\alpha +\frac{3}{4}\eta^2\cos^2 2\alpha \qquad (11)$$

$$C = -\frac{3}{8}+\frac{1}{3}\eta^2 +\frac{1}{4}\eta\cos 2\alpha -\frac{3}{8}\eta^2\cos^2 2\alpha \qquad (12)$$

- signal shapes of central transitions for different asymmetry parameters η_Q (here η) in units of $(\nu - \nu_0) / X$:

$$X = \frac{1}{9}\left|I(I+1)-\frac{3}{4}\right|\frac{\nu_Q^2}{\nu_0} \qquad (13)$$

static measurement   MAS
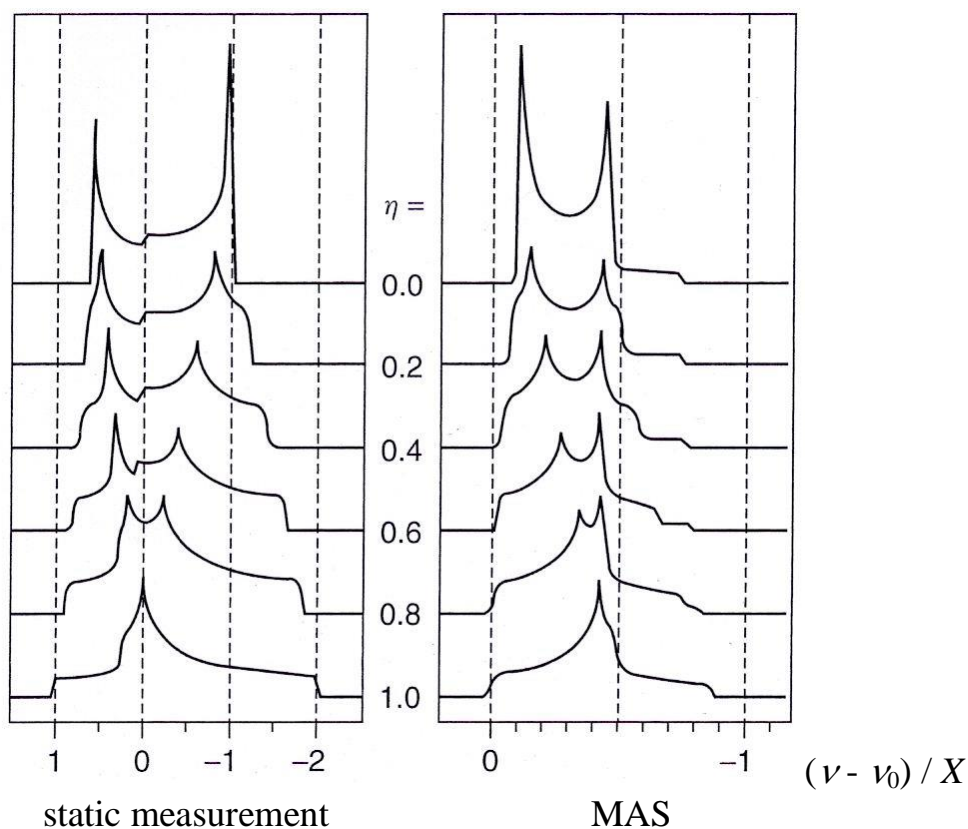
(for MAS, i.e. magic angle sample spinning, see Section 2.3)

- the centres of gravity of the central transition signals and of the satellite transition signals are shifted by the frequency difference $\Delta \nu$ [Freude1]:

$$\Delta \nu = -\frac{\nu_Q^2}{30\nu_0} 9 \cdot \left(1 + \frac{\eta^2}{3}\right) \tag{14}$$

- furthermore, the centres of gravity of the central transition signals show a field dependent (B_0 field) shift ν_{QS} (quadrupolar shift):

$$\nu_{QS} = -\frac{1}{30}\frac{\nu_Q^2}{\nu_0}\left[I(I+1)-\frac{3}{4}\right](1+\frac{1}{3}\eta^2) \tag{15}$$

Four methods for the determination of the quadrupolar interaction

1) In the case of weak quadrupolar interactions, an evaluation of the distances of the singularities of the satellite transition signals can be performed (page 4, bottom).

2) Alternatively, the difference $\Delta \nu$ of the centres of gravity of the satellite and central transition signals can be measured and evaluated (Equ. (14)).

3) In the case of strong quadrupolar interactions, a computer fit of the signal shape of the central transition can be performed (page 6, bottom).

4) If the signal has no well-defined shape, the field-dependent quadrupolar shift ν_{QS} of the central transition signal measured in different magnetic B_0 fields can be evaluated (Equ. (15)).

Benefit of the obtained spectroscopic data

- the quadrupole frequency ν_Q and asymmetry parameter η_Q give insight into the charge distribution and symmetry (electric field gradient) in the local structure of resonating quadrupolar nuclei (see also Section 3.4)
- allow to distinguish atoms located at different crystallographic positions and/or in amorphous phases

1.4   Knight Shift

- resonance shift (Knight shift) of the NMR signals of nuclei with unpaired electrons in their neighbourhood
- is also called Fermi contact interaction of these nuclei with paramagnetic centres
- Knight shift K (in ppm) or $\Delta\nu$ (in frequency units) [Fraiss1]:

$$K = \frac{\Delta\nu}{\nu_0} = \frac{a \cdot \chi_P}{\gamma_e \gamma_n \hbar} \qquad (16)$$

with the Pauli susceptibility of the unpaired electrons χ_P and the gyromagnetic ratios of electrons γ_e and the resonating nucleus γ_n

- parameter a depends on the strength of the hyperfine interaction of the resonating nucleus and the unpaired electrons
- the Knight shift Hamiltonian H_K of nuclei with spin I is:

$$H_K = \gamma_n \cdot \hbar \cdot K \cdot I \cdot B_0 \qquad (17)$$

- the Knight shift K is often stronger than the effect of the shielding σ or chemical shift and has mostly a positive sign:

$$\omega = \omega_0(1 - \sigma + K) \qquad (18)$$

- therefore, a large positive resonance shift can be a hint at the presence of metallic clusters with unpaired electrons in the neighbourhood of the resonating nuclei

Experimental evidence for Knight shift

- verification of the temperature dependence of K via the Korringa equation:

$$K^2 = \frac{\hbar}{4\pi k_B}\left(\frac{\gamma_e}{\gamma_n}\right)^2 S \frac{1}{T_1 T} \qquad (19)$$

with the spin lattice relaxation time T_1, temperature T and the scaling factor S

Benefit of the obtained spectroscopic data

- proof of unpaired electrons in the neighbourhood of resonating nuclei and their localization (see Attachment 1)

1.5 Dipole-Dipole Interaction

- Interaction of the resonating nucleus *I* with the magnetic dipole moments of neighbouring nuclei (nuclei *S*)
- the dipole moments of neighbouring nuclei cause weak magnetic fields, which overlap the external B_0 field (see bottom)
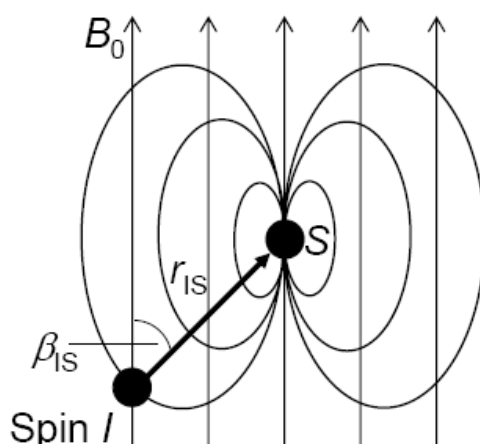
- dipole-dipole interactions depend on the nucleus-nucleus distance r_{IS} and the angle β_{IS} between the nucleus-nucleus vector and the direction the of B_0 field
- Hamiltonians of the homonuclear (same nuclei *I* with γ_I) and the heteronuclear (different nuclei *I* and *S* with $\gamma_I \neq \gamma_S$) dipole-dipole interaction $\boldsymbol{H}_{\mathrm{DI,II}}$ and $\boldsymbol{H}_{\mathrm{DI,IS}}$, respectively:

$$\boldsymbol{H}_{\mathrm{DI,II}} = \gamma_I \gamma_S \hbar^2 \frac{\mu_0}{4\pi} \frac{1}{r_{IS}^3}\left(\frac{1-3\cos^2 \beta_{IS}}{2}\right)(3I_z{\cdot}S_z - \boldsymbol{I}{\cdot}\boldsymbol{S}) \tag{20}$$

$$\boldsymbol{H}_{\mathrm{DI,IS}} = \gamma_I \gamma_S \hbar^2 \frac{\mu_0}{4\pi} \frac{1}{r_{IS}^3}\left(\frac{1-3\cos^2 \beta_{IS}}{2}\right)I_z{\cdot}S_z \tag{21}$$

- alternative description:

$$\boldsymbol{H}_{\mathrm{DI}} = \hbar \cdot \omega_{\mathrm{DI}}(A + B) \tag{22}$$

with

$$\omega_{DI} = (\gamma_i \gamma_k \hbar \frac{\mu_0}{4\pi})/r_{ik}^3 \qquad (23)$$

$$A = (1 - 3\cos^2 \beta_{ik})I_{zi}I_{zk} \qquad (24)$$

$$B = -\frac{1}{4}(1 - 3\cos^2 \beta_{ik})[I_{+i}I_{-k} + I_{-i}I_{+k}] \qquad (25)$$

Term A: distribution of the Larmor frequency due to different magnetic fields at the positions of the nuclei

Term B: flip-flop term due to spontaneous polarization transfer (spin diffusion, T_2 relaxation) between neighbouring spins

- spectra of dipolarly interacting spin pairs with $I = 1/2$ are composed by two mirrored tensors since each neighbouring nucleus S of the resonating nucleus I can have the two quantum states $m_S = \pm 1/2$

3/2 $\omega_{DI}(3\cos^2\beta_{ik}-1)$

3/2 ω_{DI}

ω_1 ω_0 ω_2

ω_0

single crystal
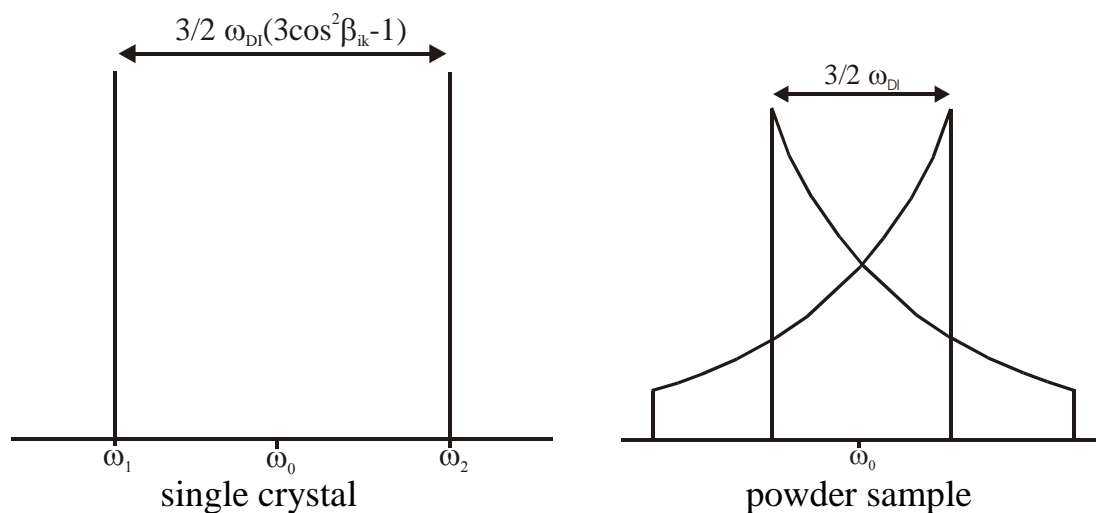
powder sample

- in the case of polycrystalline samples, the values of the angle β_{ik} covert he range of 0° to 90° and a powder spectrum occurs (see top, right), also called Pake doublet (see Attachment 2 and Section 3.2)

Benefit of the obtained spectroscopic data

- evaluation of the strength of the dipolar interactions allow the determination of nucleus-nucleus distances in crystalline as well as amorphous solids

1.6   Anisotropic Chemical Shielding and Shift

- shielding of the external B_0 field by the electron shell around the nucleus
- shielding σ is mostly anisotropic, i.e. is a tensor with $|\sigma_{zz}| \geq |\sigma_{yy}| \geq |\sigma_{xx}|$
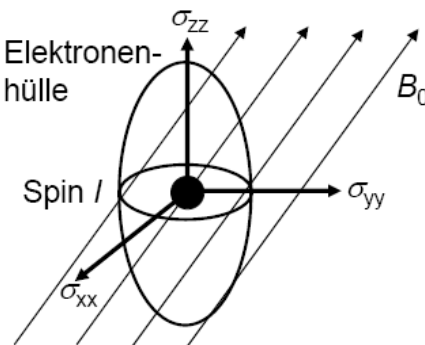
- Hamiltonian H_{CSA} of the anisotropic chemical shielding:

$$H_{CSA} = \gamma \cdot \hbar \cdot I \cdot \sigma_{\alpha\beta} \cdot B_0 \tag{26}$$

- frequency distribution function (signal shape) due to anisotropic chemical shielding:

$$\omega = \omega_0 \left[(1 - \sigma_{iso}) - \Delta\sigma \left(\frac{3\cos^2\beta - 1}{2} + \frac{\eta_{CSA}}{2} \sin^2\beta \cos 2\alpha \right) \right] \tag{27}$$

with isotropic shielding σ_{iso} (bzw. $-\delta_{iso}$):

$$\sigma_{iso} = \frac{1}{3}(\sigma_{xx} + \sigma_{yy} + \sigma_{zz}) \tag{28}$$

anisotropy $\Delta\sigma$: $\qquad \Delta\sigma = (\sigma_{zz} - \sigma_{iso}) \tag{29}$

asymmetry parameter η_{CSA}:

$$\eta_{CSA} = \frac{(\sigma_{yy} - \sigma_{xx})}{\Delta\sigma} \tag{30}$$

- in liquids, the rapid reorientation of the molecules causes an averaging of the anisotropic terms in Equ. (27):

$$\omega = \omega_0(1 - \sigma_{iso}) \tag{31}$$

- in polycrystalline solids cover the Euler angles α and β in Equ. (27) al values from 0° to 90°, which leads to the following spectra:

general case, $\eta_{CSA} \neq 0$ axial symmetry, $\eta_{CSA} = 0$
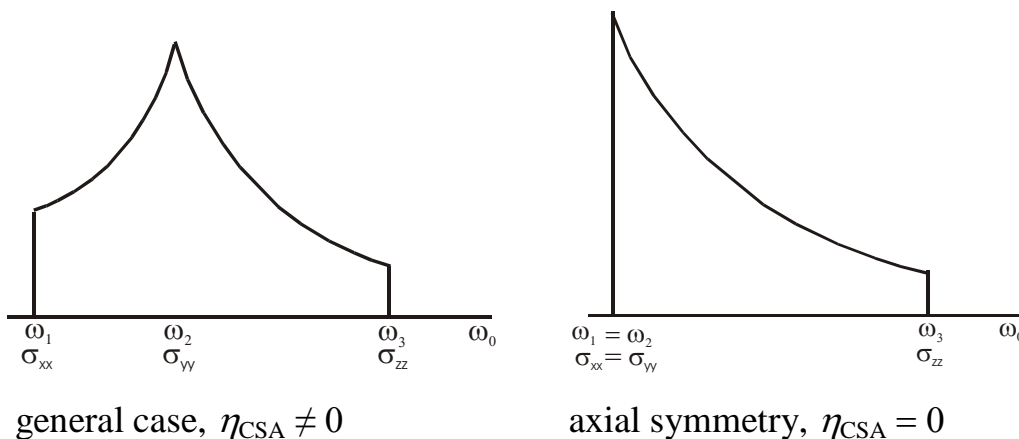
- in the case of axial symmetry ($\eta_{CSA} = 0$) is $\sigma_{xx} = \sigma_{yy}$ and often the following assignments of the principal axes values of the shielding tensor are used:

$$\sigma_{\perp} = \sigma_{zz} \tag{32}$$

$$\sigma_{\parallel} = \sigma_{xx} = \sigma_{yy} \tag{33}$$

Benefit of the obtained spectroscopic data

- the values of the anisotropy of the chemical shielding give insight into the nature and spatial arrangement of neighbouring atoms (see Attachment 3)
- support the assignment of signals in SSNMR spectra (see Section 3.3)

1.7 *J*-Coupling and Indirect Nuclear Spin-Spin Interaction

- indirect nuclear spin-spin interaction (J-coupling) is a through-bond interaction arising from interactions with bond electrons
- has a scalar value, which is independent of the strength of the magnetic B_0 field
- Hamiltonian $\boldsymbol{H}_J$ with the scalar parameter J_{ij}, which describes the through-bond interaction between the nuclei i and j:

$$\boldsymbol{H}_J = \boldsymbol{I}_i \cdot J_{ij} \cdot \boldsymbol{S}_j \tag{34}$$

- the *J*-coupling causes a signal splitting of up to 5×10^2 s^{-1}, which are, in the most cases, covered by the much broader signals in SSNMR spectra

## 2.	Experimental Techniques of Solid-State NMR Spectroscopy

## 2.1	Saturation-Free Pulse Excitation of Large Spectral Ranges

Correct pulse excitation

- radio frequency pulses (RF) with magnetic field strength B_1 causes a rotation of the magnetisation M with the nutation frequency $\omega_1 = \gamma \cdot B_1$ from the z direction (B_0 direction) into the *x-y* plane (see bottom):
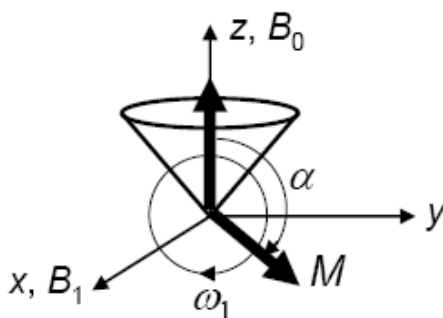
- dependent on the B_1 field strength (power of the pulse), $\omega_1/2\pi$ can reach up to 500 kHz

- the pulse length t_p as a function of the nutation angle $\alpha = \pi/2, \pi \dots$ is:

$$t_p = \frac{\alpha}{\omega_1} = \frac{\alpha}{\gamma B_1} \tag{35}$$

- the dependence of the excitation range $\Delta\nu$ (spectral excitation range) on the pulse length t_p is:

$$\Delta\nu \approx 1/(\pi\, t_p) \tag{36}$$

- spectral range, e.g., of 3 MHz (for ^{27}Al-SSNMR) requires $t_p \leq 0.1$ μs!

Preventing signal saturation

- the repetition time of NMR experiments (t_{rep}) in the case of excitation with $\pi/2$ pulses should be *ca.* $5 \times T_1$ (T_1: spin-lattice relaxation time)

- otherwise, saturation of the resonating spin system (not complete relaxation) and a loss of signal intensity would occur

- for very long T_1 times, an excitation with shorter pulses, i.e. with optimised nutation angles (Ernst angle) α_{opt} can be performed (without saturation):

$$\cos(\alpha_{opt}) = \exp\{-t_{rep}/T_1\} \qquad (37)$$

- examples of Ernst angles α_{opt} for a nuclear spin system with a T_1 time of 5 s and allowing shorter experiment repetition times t_{rep}:

t_{rep}	7.5 s	5.0 s	2.5 s
α_{opt}	77°	68°	53°

2.2   Signal Enhancement by Cross Polarization (CP)

- enhancement of signal intensities of nuclei S with low natural abundance and/or small gyromagnetic ratio (S: ^{13}C, ^{15}N, ^{29}Si etc.)

- usage of the high population difference ΔN_I at the nuclear energy levels of dipolarly coupled ^1H nuclei I for an enhancement of ΔN_S via polarization transfer from I to S spins (CP: cross polarization):

$$\frac{\Delta N_I}{\Delta N_S} = \frac{\gamma_I}{\gamma_S} \qquad (38)$$

- prerequisite for this polarization transfer is an equalization of the energy levels of the dipolarly coupled spins I and S in the magnetic field components $B_{1,I}$ and $B_{1,S}$ of long (1 to 6 ms) RF pulses (*contact pulses*)
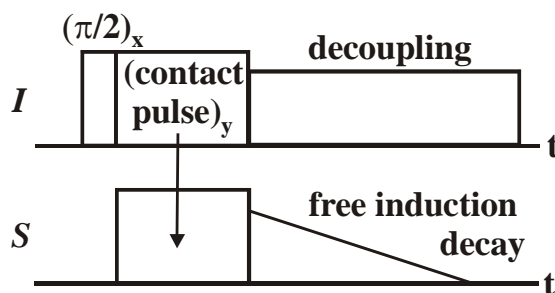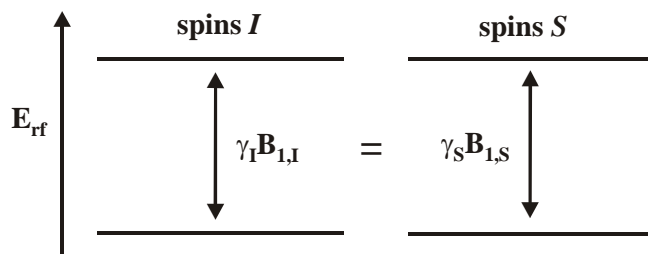
- a $\pi/2$ pulse produces I polarization and contact pulses allow the polarization transfer from spins I to neighbouring spins S if the Hartmann-Hahn condition is valid:

$$\gamma_I B_{1,I} = \gamma_S B_{1,S} \tag{39}$$

- during the detection of the NMR signal of the spins S, a weak and long decouple pulse is irradiated at the spins I for averaging dipolar I-S interactions being responsible for signal broadening

Parameters influencing the CP experiment

- the polarization $M_S(t)$ of the spins S, produced by cross polarization depends on the duration t of the contact pulses [Michel1]:
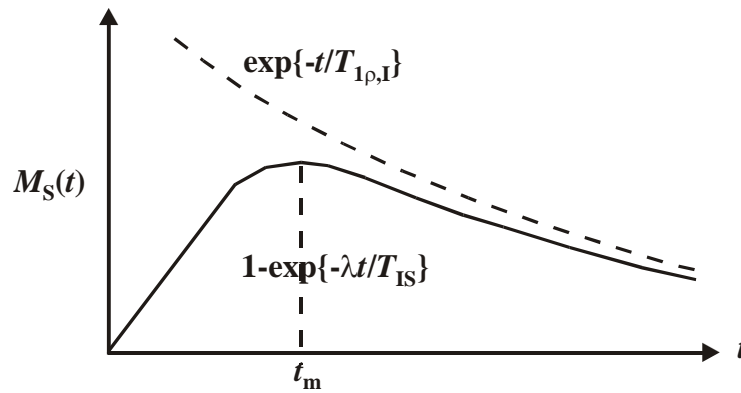
- influencing parameters are the relaxation time $T_{1\rho,I}$ of the spins I in the $B_{1,I}$-field (dashed curve), the cross polarization rate T_{IS}:

$$\frac{1}{T_{IS}} = \frac{3}{2} M_{2,IS} \left(\frac{2\pi}{5M_{2,II}} \right)^{1/2} \tag{40}$$

the second moments $M_{2,IS}$ and $M_{2,II}$ of the dipolar I-S and I-I interaction (strength of these dipole-dipole interactions) and the parameter λ:

$$\lambda = 1 + \frac{T_{IS}}{T_{1\rho,S}} - \frac{T_{IS}}{T_{1\rho,I}} \tag{41}$$

- the optimum of $M_s(t)$ is reached after the contact time t_m:

$$t_m = \frac{T_{IS} \cdot T_{1\rho,I}}{T_{1\rho,I} - T_{IS}} \cdot \ln\left(\frac{T_{1\rho,I}}{T_{IS}} \right) \tag{42}$$

Hint

- the optimum length of the contact pulses (1 bis 6 ms) is mostly experiment-tally adjusted because of the numerous parameters influencing $M_S(t)$
- since parameters in Equ. (40) to (42) are often not known, a detailed quantitative evaluation and discussion of the signal intensities is not possible

2.3 Rapid Sample Spinning Around an Axis in the Magic Angle (MAS)

- separation and evaluation of broad and overlapping SSNMR signals require application of techniques leading to a narrowing of these signals
- averaging of nuclear spin interactions rapid sample rotation (ν_{rot} of up to 60 kHz) around an axis in the angle of $\beta = 54.7^o$ related to the direction of the B_0 field (MAS: magic angle spinning)
- in this case, the term $(3\cos^2\beta - 1)$ in most of the frequency distribution functions becomes zero
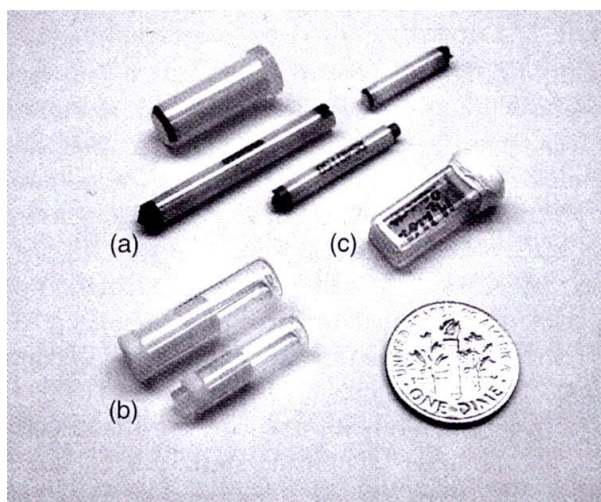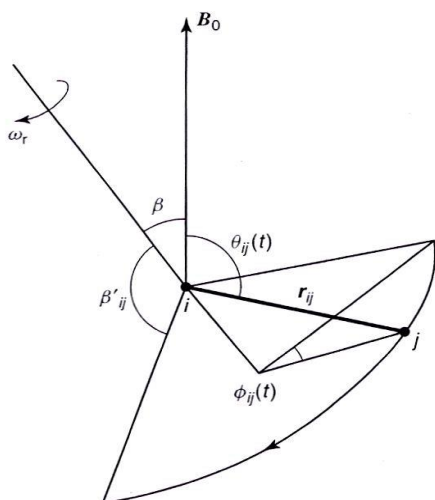
- Hamiltonian, e.g., of the dipolar *I-S* interaction under application of MAS:

$$\boldsymbol{H}_{DI, IS}(t) = \tfrac{1}{2}\, \gamma_i \cdot \gamma_j \cdot \hbar^2 \cdot r_{ij}^{-3}\, (\boldsymbol{I}_i \cdot \boldsymbol{S}_j - 3I_{iz} \cdot S_{jz}) \times$$

$$\begin{aligned}
\{ \,&(1/2)\,(3\cos^2\beta - 1) \cdot (3\cos^2\beta\,'_{ij} - 1) && \text{central line} \\
+ &(3/2)\,\sin^2\beta \cdot \sin^2\beta\,'_{ij} \cdot \cos(2\pi\nu_{rot}\cdot t + \Phi_{0ij}) && \text{sidebands} && (43) \\
+ &(3/2)\,\sin^2\beta \cdot \sin^2\beta\,'_{ij} \cdot \cos^2(2\pi\nu_{rot}\cdot t + \Phi_{0ij}) \,\} && \text{sidebands}
\end{aligned}$$

- therefore, MAS NMR spectra consist of the central line and spinning sidebands in a distance of $\pm \nu_{rot}$ relative to the central line

Rotation around an axis in the magic angle via multi-pulse sequences

- in the case of strong homonuclear dipole-dipole interaction, application of MAS can have problems with the total narrowing of the SSNMR signals
- helpful could be the irradiation a multi-pulse sequence (see bottom), e.g. in combination with MAS (CRAMPS: combined rotation and multi-pulse sequence)
- using the pulse sequence WAHUHA, the magnetization is rotated via $\pi/2$ pulses from the z (001) direction into the x (100), y (010) and back into the z direction (001)
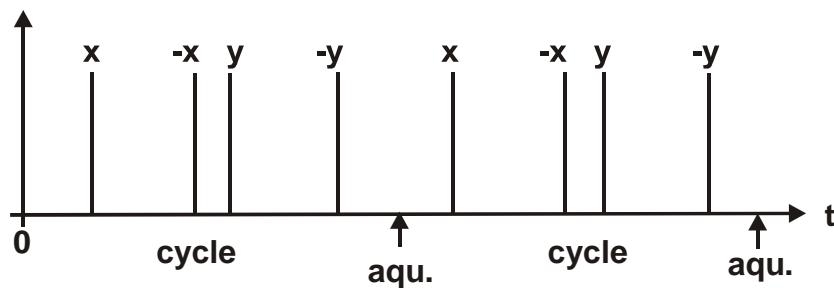
- this procedure corresponds to a rotation of the magnetization around an (111) axis, which is in the magic angle of 54.7^o to the z direction (001) [Grimmer 1]
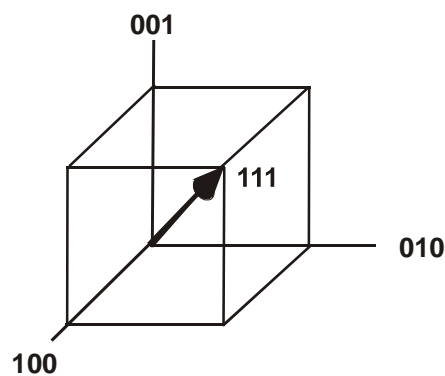
- the pulse sequence consists of a repetition of *n* cycles, in which always one data point of the induction decay is recorded (aqu.)

Limitations of MAS in the case of thermal mobility

- thermal mobility (described by correlation time τ_c) of the resonating nuclei comprise the effect of MAS and leads to a residual width $\Delta v_{1/2}{}^{MAS}$ of the central line [Andrew1]:
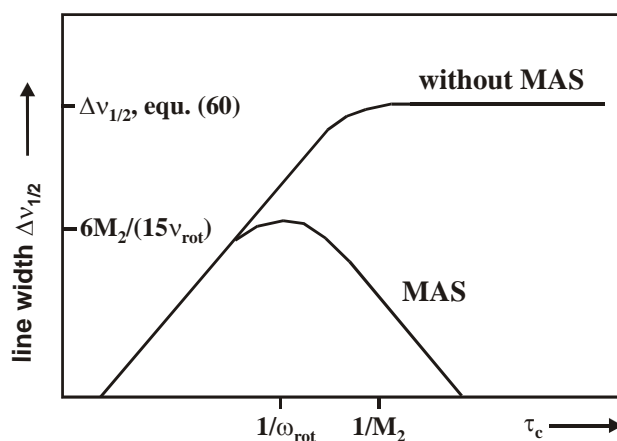
$$\Delta v_{1/2}{}^{MAS} = \frac{1}{6\pi} M_{2,IS} \left[\frac{2\tau_c}{1+(\omega_{rot}\tau_c)^2} + \frac{\tau_c}{1+4(\omega_{rot}\tau_c)^2} \right] \qquad (44)$$

- the influence of thermal mobility on the whole MAS NMR spectrum can be calculated via the following induction decay $G^{MAS}(t)$ and subsequent Fourier transformation into the frequency range [Pfeifer1]:

$$G^{MAS}(t) = \exp\{-(M_{2,IS}/3)[2J(\omega_{rot}, t)+J(2\omega_{rot}, t)]\} \qquad (45)$$

mit $\qquad J(\omega_{rot}, t)) = \dfrac{\tau_c t}{1+(\omega_{rot}\tau_c)^2} + \dfrac{\tau_c^2((\omega_{rot}\tau_c)^2-1)}{(1+(\omega_{rot}\tau_c)^2)^2}(1-e^{-t/\tau_c}\cos(\omega_{rot}t))$

$$-\frac{2\omega_{rot}\tau_c^3}{(1+(\omega_{rot}\tau_c)^2)^2} e^{-t/\tau_c}\sin(\omega_{rot}t) \qquad (46)$$

Example of signal broadening by thermal mobility

- calculated ^1H MAS NMR spectra of structural OH groups (Si(OH)Al) in zeolite H-Y (dipolar ^1H-^{27}Al interaction of $M_{2,IS} = 0.7 \times 10^{-8}$ T^2) for $v_{rot} = 3$ kHz and $\tau_c = 10$ µs to 10 ms:

The figure shows stacked spectra with correlation times τ_c of 10 μs, 100 μs, 500 μs, 1 ms, and 10 ms, ranging from "mobile" (top) to "rigid" (bottom). The horizontal axis is labeled $2\nu_{rot}$, $1\nu_{rot}$, 0, $-1\nu_{rot}$, $-2\nu_{rot}$.
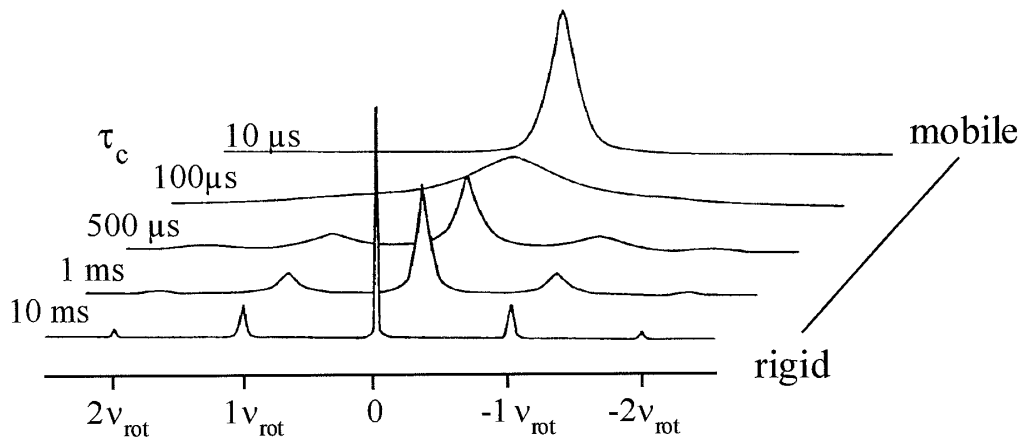
Hint

- a suitable averaging of spin interactions in solids via MAS requires $\tau_c \gg 1/\omega_{rot}$ respectively $\omega_{rot} \gg 1/\tau_c$

- therefore, helpful are high sample spinning frequencies and/or low temperature (large τ_c)

Limitations of MAS in the case of quadrupolar nuclei (S > ½)

- the effect of MAS of quadrupolar nuclei is described by the second moment $M_{2,Q}{}^{MAS}$, which is proportional to the strength of the not averaged residual quadrupolar interactions [Freude1]:

$$M_{2,Q}{}^{MAS} = \frac{1}{4}\nu_{QS}^2 \qquad \text{(for } \nu_{QS}\text{, see Equ. (15))} \tag{47}$$

- in the case of a static measurement, i.e. without MAS, the second moment of the quadrupolar interaction is:

$$M_{2,Q}{}^{statisch} = \frac{23}{7}\nu_{QS}^2 \tag{48}$$

- via Equs. (47) and (48), the narrowing of central transition signals due to MAS (proportional to the square root of M_2) can be calculated (compare with spectra on page 6, bottom):

$$\sqrt{\frac{M_{2,Q}^{MAS}}{M_{2,Q}^{static}}} = \sqrt{\frac{7}{92}} = \frac{1}{3.6} \approx \frac{1}{4} \tag{49}$$

2.4 Complete Averaging of Quadrupolar Interactions via Sample Around Two Axes (DOR)

- in the case of using the quantum level p with $p/2 \leftrightarrow -p/2$ instead of $m \leftrightarrow -m$, the frequency distribution function of the central transition signal $\nu_{p/2,-p/2}$ during application of MAS is [Freude1]:

$$\nu_{p/2,-p/2} = \nu_{p/2,-p/2}^{\text{iso}} + \nu_{p/2,-p/2}^{\text{aniso}}$$

$$= \frac{p\nu_Q^2(3+\eta^2)}{90\nu_0}\left\{I(I+1) - \frac{3}{4}p^2\right\} - \left\{\frac{p\nu_Q^2}{12960\nu_0}\right\} \tag{50}$$

$$\times \left\{(18+\eta^2)d_{0,0}^{(4)} + \sqrt{360} \cdot \eta \cdot d_{2,0}^{(4)} \cdot \cos 2\alpha + \sqrt{70} \cdot \eta^2 \cdot d_{4,0}^{(4)} \cdot \cos 4\alpha\right\}$$

$$\times \left\{36I(I+1) - 17p^2 - 10\right\}\left\{(-\frac{9}{28}) \cdot (35\cos^4\beta - 30\cos^2\beta + 3)\right\}$$

- averaging of term $\nu_{p/2,-p/2}^{\text{aniso}}$ if $\beta = 30.56^\circ$ or 70.12° ($35\cos^4\beta - 30\cos^2\beta + 3 = 0$), i.e., for sample spinning around a second axis in the angle β (DOR: double oriented rotation).
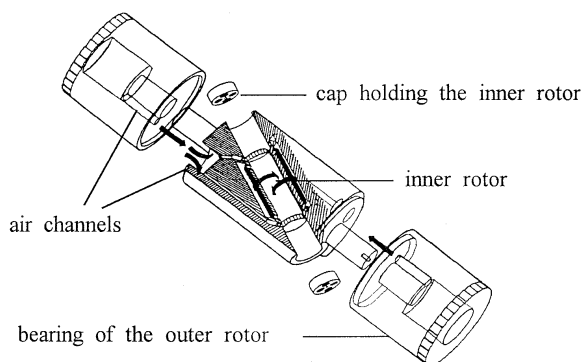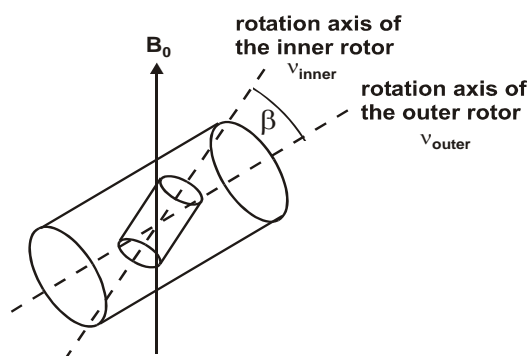
- the small inner rotor containing the sample can rotate with ν_{rot} ca. 6 to 8 kHz, while the large outer rotor reaches ca. 2 kHz

Limitations of the DOR technique

- low signal/noise ratio due to low coil filling factor
- numerous spinning sidebands due to small ν_{rot} of outer rotor

2.5 Complete Averaging of Quadrupolar Interactions due to Multiple-Quantum NMR Experiments (MQ)

- combination of MAS with pulse sequences (echo sequence) for eliminating the residual signal width of the central transition of quadrupolar nuclei
- excitation of MQ transitions m_1 (MQ: multiple-quantum) via a strong pulse, MQ evaluation time t_1, and signal detection during the period t_2 after conversion into single-quantum transitions m_2 via weak pulses [Frydman 1]
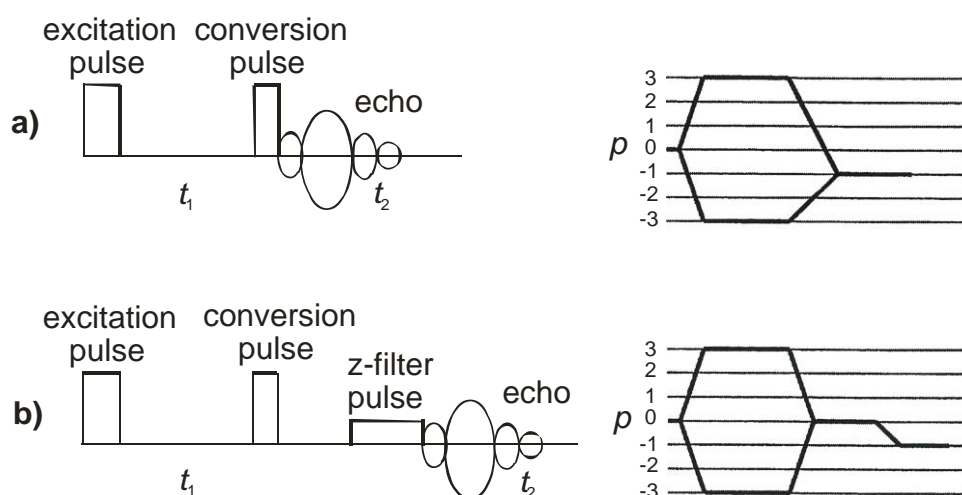
- conditions for t_1 und t_2 in the pulse sequences show above [Frydman1]:

$$t_1\, C_4(m_1)\ +\ t_2\, C_4(m_2)\ =\ 0 \tag{51}$$

with $C_4(m_1) = -42$ und $C_4(m_2) = 54$ for nuclei with spin $I = 3/2$ and $C_4(m_1) = -300$ and $C_4(m_2) = 228$ for nuclei with spin $I = 5/2$

- recording of the echo signals $G(t_1,t_2)$ at the time $t_{2,\text{echo}}$:

$$t_{2,\text{echo}} = [|C_4(m_1)|/C_4(1/2)]\, t_1 \tag{52}$$

- twofold Fourier transformation (FT) of the echo signals $G(t_1,t_2)$ as a function of the MQ evaluation time t_1 gives a two-dimensional (2D) MQMAS NMR spectrum

- 2D MQMAS NMR spectra show quadrupolar influenced MAS NMR signals along the δ_2 axis (FT of t_2) and fully isotropic signals (quadrupolar interactions completely averaged) along the δ_1 axis (FT of t_1).

Limitations of the MQMAS NMR technique

- MQ pulse sequences can be optimized for a limited range of C_q values only
- signal intensities of 2D MQMAS NMR spectra cannot be evaluated in a quantitative manner

Example for the application of the MQMAS NMR technique

- 2D MQMAS NMR spectrum of ^{17}O atoms in Si^{17}OSi (80%, $C_Q = 5.3$ MHz) and Si^{17}OAl bridges (20%, $C_Q = 3.5$ MHz) of a crystalline aluminosilicate [Freude 1]
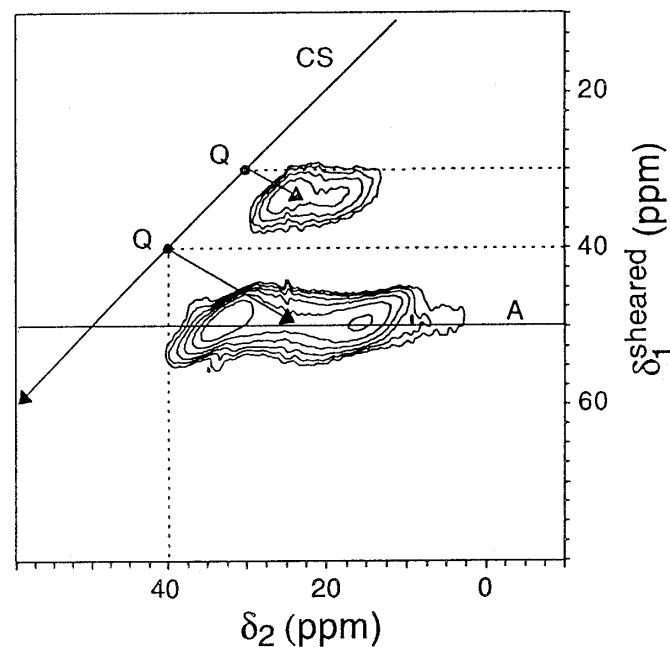
3. Applications

3.1 Determination of the Framework n_{Si}/n_{Al} Ratio of Crystalline Aluminosilicates via ^{29}Si HPDEC MAS NMR

The isotropic chemical shift δ_{Si} of ^{29}Si atoms (^{29}Si: spin $I = 1/2$) of crystalline aluminosilicates depends in a characteristic manner on the type and number of atoms at the directly neighboured T positions (see bottom).

```
      Al            Al            Al            Al            Si
      O             O             O             O             O
  AlO SiOAl     AlOSiOSi     SiOSiOSi     SiOSiOSi     SiOSiOSi
      O             O             O             O             O
      Al            Al            Al            Si            Si


    Si(4Al)       Si(3Al)       Si(2Al)       Si(1Al)       Si(0Al)
```
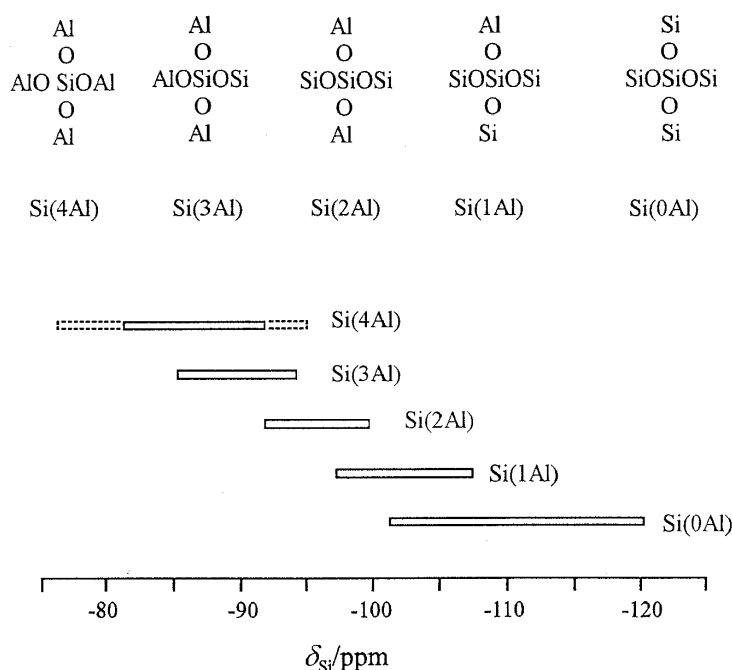

Therefore, the lattice n_{Si}/n_{Al} ratio n these crystalline solids can be calculated by the relative intensities $I_{Si(nAl)}$ of the ^{29}Si MAS NMR signals of the Si(nAl) species via:

$$n_{Si}/n_{Al} = \sum_{n=0}^{4} I_{Si(nAl)} / \sum_{n=0}^{4} 0.25 \cdot n \cdot I_{Si(nAl)} \tag{53}$$

This method allows the investigation of changes in the lattice n_{Si}/n_{Al} ratio, e.g., due to dealumination procedures or catalytic applications.

For studying the aluminum content of the lattice of a crystalline aluminosilicate, ^{29}Si MAS NMR measurements were performed at $B_0 = 9.4$ T

corresponding to $\nu_0 = 79.4$ MHz, with single-pulse excitation ($\pi/2$), ^{1}H high power decoupling (HPDEC) and $\nu_{rot} = 4$ kHz.

For the evaluation, the ^{29}Si HPDEC MAS NMR spectrum was decomposed in the signal components and their relative intensities $I_{Si(nAl)}$ were determined. The calculation of the lattice n_{Si}/n_{Al} ratio via Equ. (53) gave $n_{Si}/n_{Al} = 2.73$.
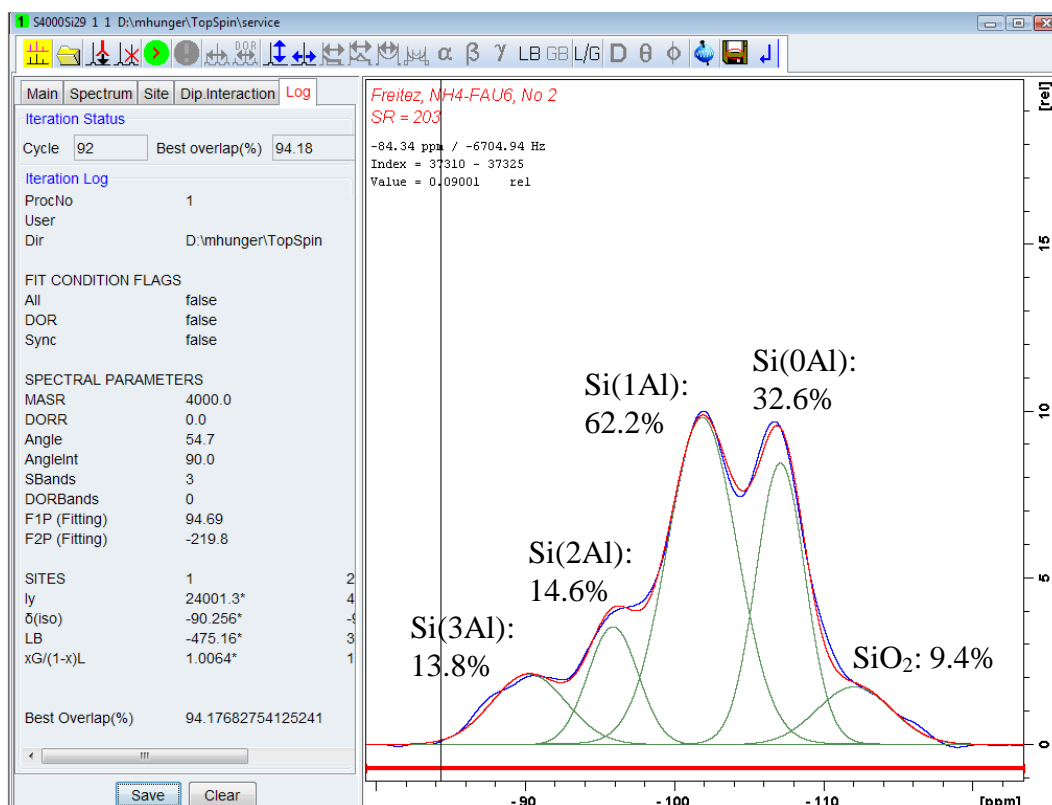
3.2 Determination of the H-H Distance of Crystal Waster in Gypsum via ^{1}H Solid-State NMR

Gypsum crystals ($CaSO_4 \cdot 2H_2O$) contain strongly bound isolated water molecules. The statically recorded ^{1}H NMR spectrum of these water molecules consists of a Pake doublet (^{1}H: spin $I = 1/2$). Via the distance of the singularities of this doublet, the H-H distance r_{HH} inside the water molecule can be determined (see Section 1.5). For the investigation of this H-H distance, an ^{1}H

echo NMR spectrum was recorded at $B_0 = 9.4$ T corresponding to $\nu_0 = 400.1$ MHz and with a pulse delay of 10 μs.

The evaluation of the distance of the Pake doublet singularities in the ^{1}H echo NMR spectrum gave a value of 113 ppm. The H-H distance r_{HH} was calculated via Equ. (23) using $\gamma_H = 2.675 \cdot 10^8$ m^{2}V^{-1}s^{-2}, $\hbar = 1.054589 \cdot 10^{-34}$ VAs^2, and $\mu_0 = 1.2566 \cdot 10^{-6}$ VsA^{-1}m^{-1}. The H-H distance of $r_{HH} = 1.585$ Å obtained by this way is in good agreement with the value of 1.533 Å determined by X-ray diffraction.
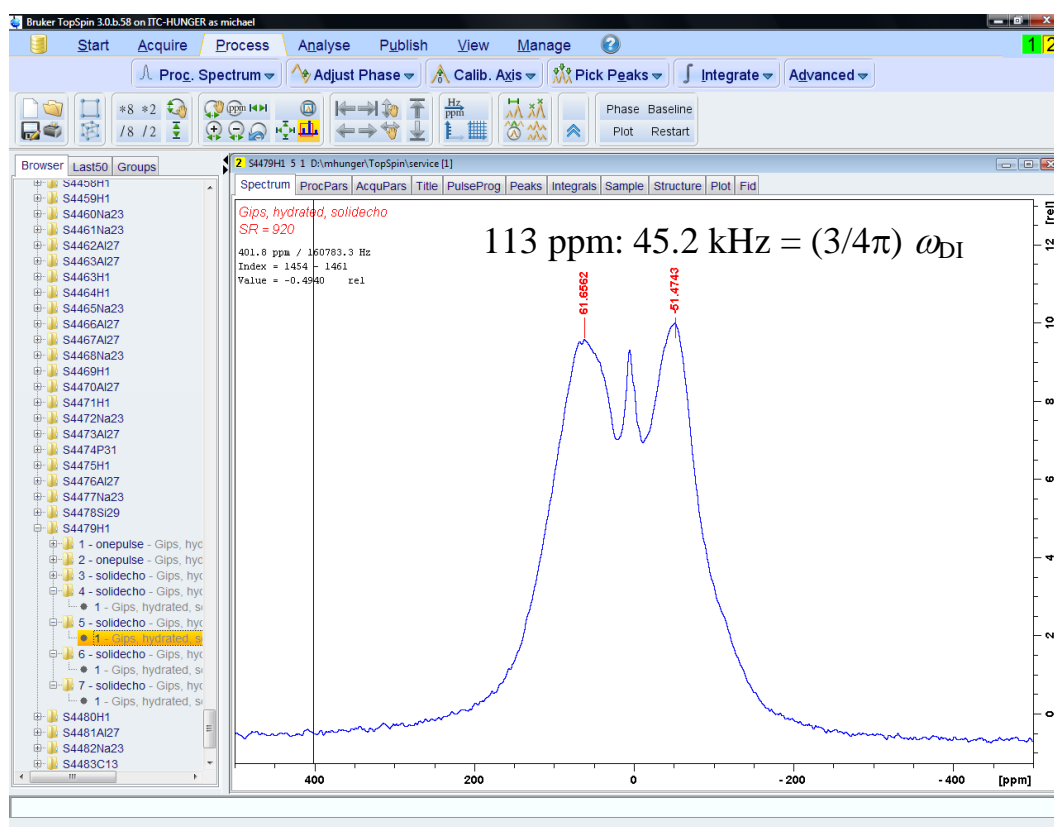
3.3 Determination of the ^{13}C Shielding Parameters of Glycine via ^{13}C CP MAS NMR

Glycine (NH$_2$CH$_2$COOH) is a solid material at room temperature (melting point 232 to 236°C). Using the cross polarization (CP) technique in combination with the rapid sample spinning around an axis in the magic angle (MAS), it is

possible to record ^{13}C solid-state NMR spectra (^{13}C: spin $I = 1/2$) of glycine with natural abundance of the ^{13}C isotope in an order of few minutes.

For studying glycine, a ^{13}C CPMAS NMR spectrum was recorded at $B_0 = 9.4$ T corresponding to $\nu_0 = 100.6$ MHz, with a contact pulse of 4 ms, and $\nu_{rot} = 2$ kHz.

$$\delta_{iso,1} = 173.5 \text{ ppm}$$
$$\delta_{iso,2} = 42.5 \text{ ppm}$$
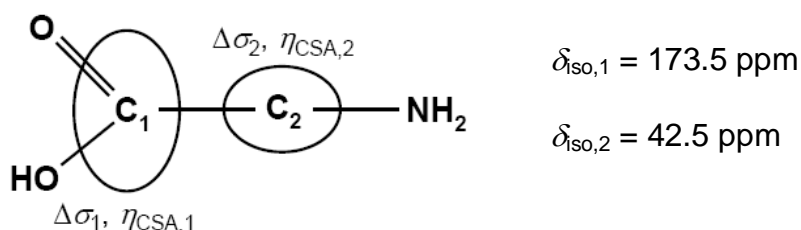
The simulation of the ^{13}C CPMAS NMR sideband pattern of glycine delivered anisotropies of the chemical shielding of $\Delta\sigma_1 = -67.7$ ppm and $\Delta\sigma_2 = 16.1$ ppm and asymmetry parameters of $\eta_{CSA,1} = 0.9$ and $\eta_{CSA,2} \approx 0$. These very different values of the shielding parameters for C1 and C2 (see Scheme on top) agree very well with the different symmetries of the local structures of these carbon atoms.

3.4 Investigation of the Na$^+$ Population in Dehydrated Zeolite Na-Y via ^{23}Na MAS NMR

In zeolite Na-Y, the negative framework charges in the local structure of framework aluminum atoms are compensated by extra-framework Na$^+$ cations (^{23}Na: spin $I = 3/2$). These Na$^+$ cations can be located in the centre of hexagonal prisms (SI, see below) or in front of a 6-ring window (SI', SII, see below). At these crystallographic positions, the Na$^+$ cations are involved in very different quadrupolar interactions (QCC corresponds to C_q).

SI SI', SII

QCC = 0-0.5 MHz QCC = 3.4-5.6 MHz
⇓ ⇓
low-field line A high-field pattern B
corresponds to SI corresponds to SI' and SII

For studying the population of the Na$^+$ sites in dehydrated zeolite Na-Y, a ^{23}Na MAS NMR spectrum was recorded at $B_0 = 9.4$ T corresponding to $\nu_0 = 105.8$ MHz, with single-pulse excitation ($\pi/6$), $\nu_{rot} = 12$ kHz.

The simulation of this ^{23}Na MAS NMR spectrum delivered quadrupole coupling constants $C_{Q,1}$ and $C_{Q,2}$ of 0.9 MHz (SI) and 3.9 MHz (SI', SII), and relative intensities of $I_1 = 29.5$ % (SI) and $I_2 = 70.5$ % (SI', SII). The above-mentioned relative intensities correspond to the Na$^+$ population ratio of the cation positions SI and SI'+SII, respectively, in dehydrated zeolite Na-Y.

4. Literature

[Andrew1]   E.R. Andrew, A. Jasinski, J. Phys. C 4 (1971) 391.

[Freude1]   D. Freude, Quadrupolar Nuclei in Solid-state Nuclear Magnetic
                Resonance, in: Encyclopedia of Analytical Chemistry, R.A, Meyers
                (Ed.), Wiley, New York, Chichester, 2000, pp. 12188-12224.

[Fraiss1]   J. Fraissard, R. Vincent, C. Doremieux, J. Kärger, H. Pfeifer,
                Application of NMR Methods to Catalysis, in: Catalysis, Science and
                Technology, J.R. Anderson, M. Boudart (eds.), Springer-Verlag, Berlin,
                Heidelberg, 1996, pp. 1-176.

[Frydman1]   L. Frydman, J.S. Harwood, Isotropic Spectra of Half-integer
                Quadrupolae Spins from Bidimensional Magic-angle Spinning NMR, J.
                Am. Chem. Soc. 117 (1995) 5367.

[Grimmer1]   A.-R. Grimmer, B. Blümich, Introduction to Solid-state NMR, in:
                Solid-state NMR II – Iorganic Matter, NMR Basic Principles and
                Progress, Vol. 30, Springer-Verlag, Berlin, Heidelberg, 1994, pp. 1-62.

[Michel1]   D. Michel, F. Engelke, NMR Basic Principles and Progress, Vol. 32,
                Springer-Verlag, Berlin, Heidelberg, 1995, pp. 69-125.

[Pfeifer1]   H. Pfeifer, NMR Basic Principles and Progress, Vol. 31, Springer-
                Verlag, Berlin, Heidelberg, 1994, pp. 32-90.

[Rose1]   M.E. Rose, Elementary Theory of Angular Momentum, Wiley, New
                York, Chichester, 1967.

Attachment 1

Knight Shift of NMR Signals of ^{29}Si and ^{27}Al Nuclei in the Neighbourhood of Paramagnetic Centres

Hyperfine interactions between unpaired electrons and framework atoms in aluminosilicate sodalites containing paramagnetic Na$_4^{3+}$ clusters: a ^{29}Si and ^{27}Al MAS NMR study
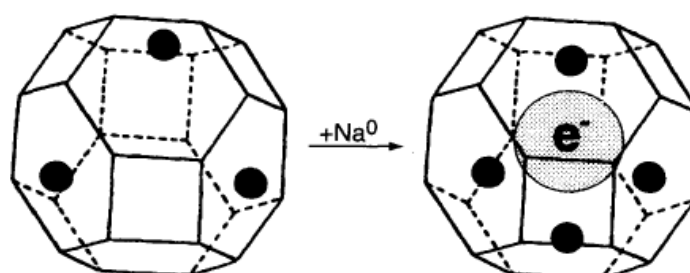
G. Engelhardt et al., Chem. Commun, 1996, 729

Fig. 1 Sodalite cages containing diamagnetic Na$_3^{3+}$ (left cage) and paramagnetic Na$_4^{3+}$ clusters (right cage). Alternating Si and Al atoms at the vertices of the cage structure are interconnected by oxygen atoms which are omitted for clarity. Black circles represent Na$^+$ cations located above the centres of the six-rings.
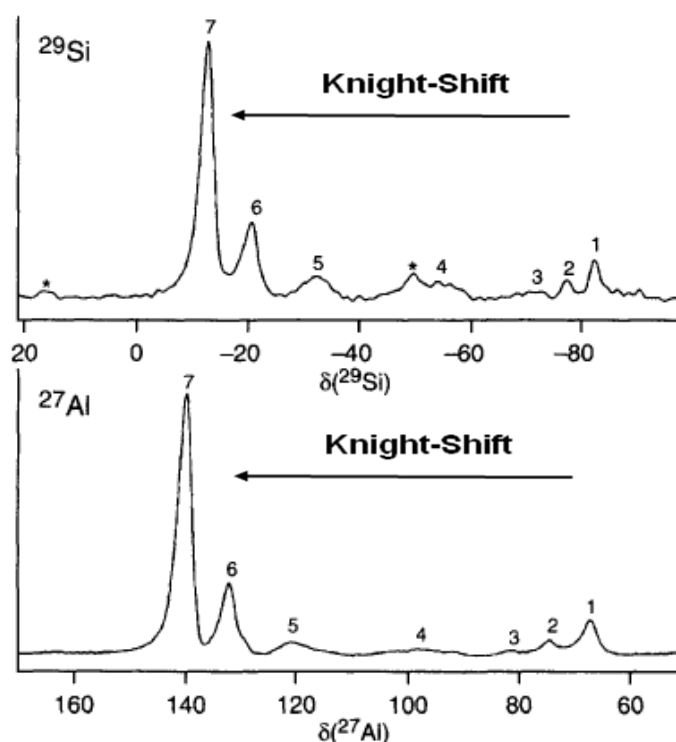

Fig. 2 ^{29}Si and ^{27}Al MAS NMR spectra of black sodalite at 295 K. Spinning speeds, pulse widths, pulse delays, and number of scans were 10 kHz, 0.7 μs, 0.5 s, and 400 for ^{27}Al, and 3 kHz, 3 μs, 10 s, and 1000 for ^{29}Si, respectively. * Denotes spinning side bands.

Attachment 2

Composition of a Pake Doublet of Nuclei *I* in the whole Range of β_{ik} Angles and via Mirror Imaging of the two Tensors for $m_S = \pm 1/2$ of the Neighboured Nuclei *S*
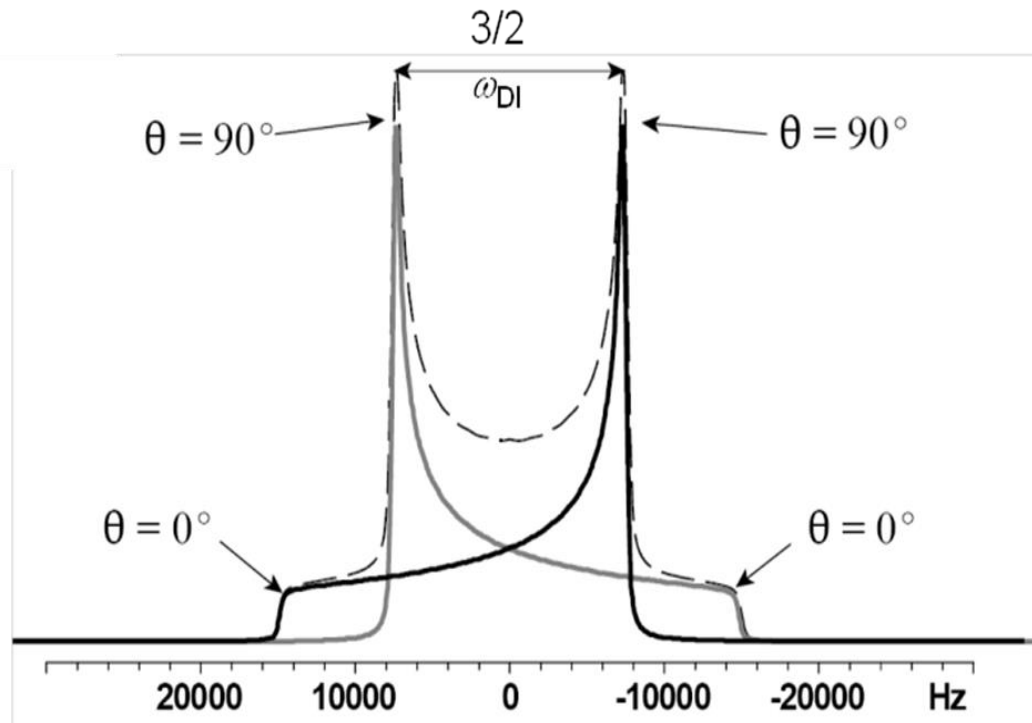
Attachment 3

Influence of the Local Structure and Local Bonds on the Principal Axis Values of the Shielding Tensor of ^{13}C Nuclei

spherical symmetry: same shielding values σ_{ii} in all directions

non-axial symmetry: different shielding values σ_{ii} in all directions

axial symmetry: shielding values σ_{ii} in two direction are equal